Energy & Environmental Science

COMMUNICATION

View Article Online
View Journal

Cite this: DOI: 10.1039/c6ee03145e

Received 26th October 2016,
Accepted 19th January 2017

DOI: 10.1039/c6ee03145e

rsc.li/ees

A general approach to cobalt-based homobimetallic phosphide ultrathin nanosheets for highly efficient oxygen evolution in alkaline media†

Xiaofen Xiao,‡[a] Chun-Ting He,‡[b] Shenlong Zhao,[c] Jing Li,[a] Wensheng Lin,[a] Zhongke Yuan,[a] Qiang Zhang,[d] Shuangyin Wang,[e] Liming Dai*[f] and Dingshan Yu*[a]

A general and effective approach was proposed to fabricate a new family of Co-based bimetallic phosphide ultrathin nanosheets (CoM-P-NS, M = Ni, Mn, Cu, Zn) with homogeneous composition and unique porous architecture using ultrathin metal–organic framework nanosheets (MOFNs) as precursors for the first time, which yielded synergistically active sites, mass transport and dynamic modulations for the oxygen evolution reaction (OER). The optimized samples showed remarkable oxygen evolution activity in alkaline electrolytes, outperforming both the commercial RuO_2 and Ir/C benchmarks and ranking the best among all the metal-phosphide electrocatalysts reported to date.

The oxygen evolution reaction (OER) is a pivotal process for diverse energy conversion and storage technologies, such as rechargeable metal-air batteries, regenerative fuel cells, and electrochemical water splitting.[1] Due to the sluggish kinetics intrinsically associated with the OER, the overall energy storage and energy (fuel) generation efficiency is often low. Ruthenium and iridium oxides are well-known to be efficient for the OER. However, their high cost and scarcity have severely impeded their large-scale applications.[2,3] Thus, there is a pressing need to develop cost-effective and highly-efficient non-noble-metal alternatives for the OER.[4–7] To this end, nanostructured transition metal phosphides have emerged as a new family of OER catalysts.[8–12] Although some progress has been achieved in exploiting monometal phosphide nanostructures (such as CoP[13,14] and Ni_2P[15,16]) for efficient OER, their performance is still far from satisfactory. Some recent studies demonstrated that the incorporation of foreign metal atoms with similar electron configuration into the crystal lattice can dramatically enhance the electrocatalytic activities of transition-metal-based materials.[17–20] It is believed that the local coordination environment and electronic structure can be expediently tuned by the doping content of an

Broader context

Two dimensional (2D) ultrathin sheet-like crystal nanostructures have been widely recognized as promising materials for a range of energy applications due to their unusual structural, electronic and physiochemical properties relative to their bulk counterparts. Inspired by the intriguing features associated with bimetallic phosphides such as abundant natural resources, tunable electronic structures, and excellent catalytic potential, concurrently fabricating and engineering ultrathin 2D bimetallic phosphides may offer a new family of low-cost electrocatalysts to replace commercial noble metal catalysts for various energy systems, yet it remains a huge synthetic challenge. Herein, we have, for the first time, established an effective and general approach for fabricating a new family of Co-based bimetallic phosphide ultrathin nanosheets (CoM-P-NS, M = Ni, Mn, Cu, Zn) with homogeneous composition as well as a tunable Co/M ratio using metal organic framework nanosheets as the precursors. The proposed approach yielded synergistically structural, compositional, and electronic modulations in bimetallic phosphide catalysts, leading to the simultaneous improvement of the active site and mass transport as well as the energetics for the oxygen evolution reaction (OER). As such, the optimized bimetallic phosphide catalysts showed remarkable OER activity in alkaline electrolytes, outperforming both the commercial RuO_2 and Ir/C benchmarks and ranking the best among all the metal-phosphide electrocatalysts reported to date. The proposed strategy of coordinated modulation is expected to broaden our horizons in designing novel highly-active noble-metal-free electrocatalysts for the OER. The facile and general synthetic methodology developed herein will pave the way to new techniques for synthesizing various other 2D sheet-like monometallic and bimetallic compounds, which will not only enrich the 2D material family but also significantly promote their practical use in a range of energy and environment-related applications.

[a] Key Laboratory for Polymeric Composite and Functional Materials of Ministry of Education, Key Laboratory of High Performance Polymer-based Composites of Guangdong Province, School of Chemistry, Sun Yat-Sen University, Guangzhou 510275, China. E-mail: yudings@mail.sysu.edu.cn
[b] MOE Key Laboratory of Bioinorganic and Synthetic Chemistry, School of Chemistry, Sun Yat-Sen University, Guangzhou 510275, China
[c] Laboratory for Nanosystem and Hierarchy Fabrication, National Center for Nanoscience and Technology, Beijing 100190, China
[d] Beijing Key Laboratory of Green Chemical, Reaction Engineering and Technology, Department of Chemical Engineering, Tsinghua University, Beijing, 100084, China
[e] State Key Laboratory of Chem/Bio-Sensing and Chemometric, College of Chemistry and Chemical Engineering, Hunan University, Changsha, 410082, China
[f] Department of Macromolecule Science and Engineering, Case Western Reserve University, Ohio, 44106, USA. E-mail: liming.dai@case.edu

† Electronic supplementary information (ESI) available. See DOI: 10.1039/c6ee03145e

‡ The authors contributed equally to this work.

additional metal, which in turn regulates the catalytic activity of these transition metal catalysts. In particular, some theoretical work pointed out that homogeneous binary-transition-metal compounds free from the undesired phase segregation are favourable to effectively modulate their 3d electronic structures to ameliorate the kinetics for better electrocatalytic performance.[20–24] Despite the great promise, there are only very few reports on nanostructured bimetallic phosphides, like CoFeP and CoMnP nanoparticles/or nanorods, which have been produced by reacting pre-synthesized metal oxide particles or highly poisonous transition metal–carbonyls with an organic phosphine at high temperature.[21–23] To date, controlled synthesis of multimetallic phosphides is still a very challenging task, because of the uncontrolled formation of multiple segregated phases arising from the difference in the reactivities of the two metal precursors as well as the stringent requirement to precisely control the stoichiometric ratio for valence balance.

To develop highly efficient electrocatalysts, the material morphology, apart from their composition, needs to be optimized to have a large surface area with numerous exposed active sites and porous network architecture for rapid transport of electrons/ions.[25–29] In this context, two-dimensional (2D) ultrathin nanosheets are particularly attractive for electrocatalysis. This is because an ultrathin 2D nanosheet can not only provide a high specific surface area to expose a large number of surface active sites as well as large-area and intimate contact with both the electrolyte and electrode for rapid interfacial charge transfer, but also render more exposed interior atoms as highly active sites through surface reorganization.[30–34] In light of the above consideration, we envision that, through rational structural engineering with ultrathin sheet-like nanostructures as well as proper composition and electronic modulation with homogeneous doping of a secondary metal, the electrocatalytic activity of transition-metal-phosphide catalysts would be further improved to a much higher level. However, relative to their extraordinary potential, 2D ultrathin nanosheet-like homogeneous bimetallic phosphide nanostructures, with abundant active sites, high surface area, and favourable electronic configuration remain a huge synthetic challenge. The lack of proper bimetallic nanosheet precursors as well as the effective control of well-defined morphologies poses major impediments to progress. Thus, it is highly desirable to develop new effective strategies for concurrently fabricating and structuring ultrathin 2D homobimetallic phosphides, which will not only enrich the 2D material family but also greatly promote their practical use in a range of energy and environment-related applications.

Herein, we report a general, but facile and controllable, approach to a new class of 2D Co-based bimetallic phosphide ultrathin nanosheets (CoM-P-NS, M = Ni, Mn, Cu, Zn) with single phase and homogenous composition by low-temperature phosphorization of bimetallic metal–organic framework nanosheet (MOFN) precursors, derived from ion-assisted solvothermal treatment of doped zeolitic imidazolate frameworks (ZIFs) (Fig. 1). To our knowledge, this is the first time that bimetallic MOFNs have been used as precursors/templates to produce a series of nanosheet-like Co-based homobimetallic phosphides. Interestingly,

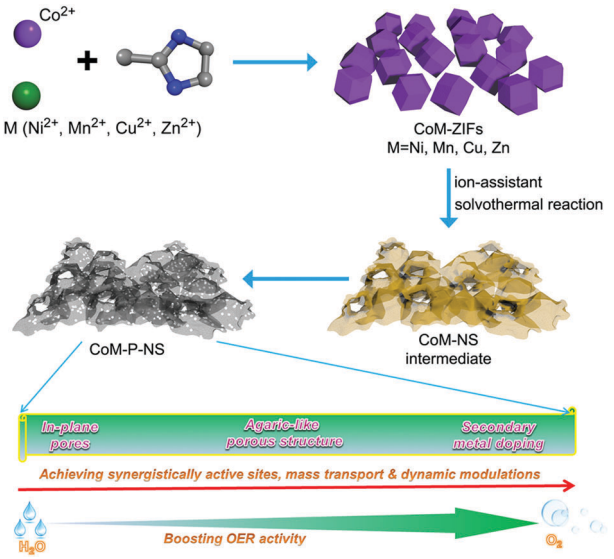

Fig. 1 Schematic illustration of a general approach to CoM-P nanosheets for highly-efficient OER derived from bimetallic MOFNs.

the phosphorization treatment induces the formation of in-plane pores on individual CoMP nanosheet surfaces, while these nanosheets as building blocks are interconnected with each other into three-dimensional agaric-like porous structures. Furthermore, secondary metals are homogeneously incorporated into the primitive CoP crystal to effectively modulate the electronic structure to optimize the binding energies of OER intermediates, as predicted by our computational studies. As expected, our proposed approach simultaneously realized effective nanostructure engineering, and compositional and electronic modulation, achieving synergistically active sites, mass transport and dynamic regulations (Fig. 1). The resultant CoM-P-NS exhibited remarkable electrocatalytic activities towards the OER in alkaline electrolyte. More impressively, the optimized CoNi-P-NS achieved an unexpectedly low overpotential of 209 mV at 10 mA cm^{-2}, outperforming all the transition-metal-phosphide electrocatalysts reported to date and the commercial RuO_2 and Ir/C benchmarks (Tables S1 and S2, ESI†). Our combined experimental and computational studies revealed the combined role of the structural, compositional and electronic modulations in contributing to the observed high catalytic activity (*vide infra*).

Fig. 1 schematically illustrates the general approach to CoM-P-NS. In a typical experiment, homogenous bimetallic ZIFs (denoted as CoM-ZIF, M = Ni, Mn, Cu, Zn) were first prepared through a fast co-precipitation reaction of a mixture of $Co(NO_3)_2{\cdot}6H_2O/M(NO_3)_2{\cdot}6H_2O$ and 2-methyl imidazole in methanol. The strong coordination of imidazole with diverse metal ions as well as the similar ionic radius in crystals and electronegativity of the dopant ions of M^{2+} with those of Co^{2+} make the homogeneous incorporation of M^{2+} into the CoM-ZIF framework possible (Fig. 2a and Table S3, ESI†).[35,36] The X-ray diffraction (XRD) profiles given in Fig. S1 (ESI†) show similar diffraction patterns for all CoM-ZIFs. Scanning electron microscopy (SEM) images reproduced in Fig. 2b and Fig. S2 (ESI†), reveal that all the resultant ZIF samples consist of uniform

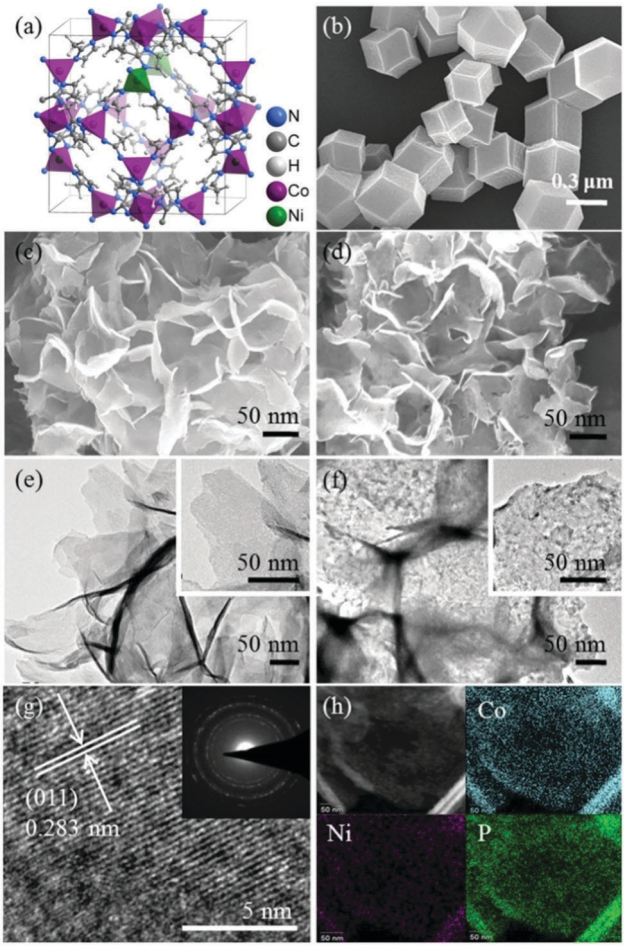

Fig. 2 (a) The crystal structure and (b) SEM image of CoNi(20 : 1)-ZIF precursor; (c) SEM and (e) TEM images with different magnifications of CoNi(20 : 1)-NS intermediates; (d) SEM, (f) TEM, (g) HRTEM images (the inset is the SAED pattern) and (h) STEM image and elemental mapping data of CoNi(20 : 1)-P-NS. Co is shown in blue, Ni in purple, and P in green.

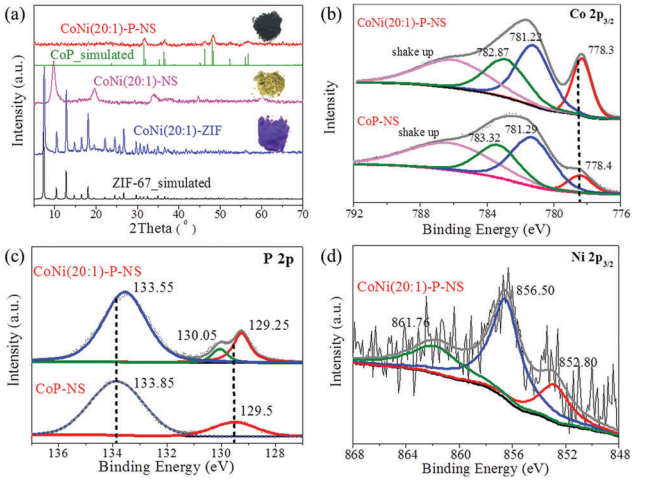

Fig. 3 (a) XRD patterns of CoNi(20 : 1)-ZIF, CoNi(20 : 1)-NS, and CoNi(20 : 1)-P-NS (the inset is the corresponding picture of the solid samples); high resolution XPS spectra of (b) Co $2p_{3/2}$, (c) P 2p and (d) Ni $2p_{3/2}$ in CoNi (20 : 1)-P-NS.

polyhedra with regular rhombic dodecahedral morphology and an average size of about 500 nm. Subsequent solvothermal reaction in the presence of Co^{2+} and M^{2+} led to a distinctive morphology evolution of the parent bimetallic ZIF from a rhombic dodecahedron to an intriguing agaric-like porous structure consisting of numerous ultrathin nanosheets (CoM-NS, Fig. 2c and Fig. S3a, ESI†). The structural evolution was confirmed by XRD profiles (Fig. 3a and Fig. S3b, ESI†), which show the disappearance of the peak at 7.4° characteristic of the parent CoM-ZIF with a concomitant appearance of three distinctive diffraction peaks at 10.2°, 20.1° and 34.2° for the newly-developed CoM-NS, as is the case for hollow Zn/Co ZIF particles.[35] The obvious colour change from purple to yellow further evidenced the structural evolution from CoNi-ZIFs to CoNi-NS (Fig. 3a).

Finally, the CoM-NS was transformed into CoM-P-NS *via* phosphorization treatment with NaH_2PO_2 at 300 °C. Although the final CoM-P-NS product became black (Fig. 3a), the agaric-like morphology consisting of nanosheets was still evident after phosphorization (Fig. 2d, f and Fig. S4–S6, ESI†). The thickness of the CoNi-P-NS is approximately 3.6 nm according to atomic force microscopic (AFM) observations (Fig. S6c, ESI†). These interconnected nanosheets acted as building blocks to form a three-dimensional porous structure, which could not only facilitate the accessibility of electrolyte and accelerate ion diffusion but also render highly exposed active sites to promote the catalytic performance. Previously reported transition-metal-phosphide electrocatalysts with morphologies of zero-dimensional nanoparticles and one-dimensional nanorods tend to be easily agglomerated,[21–23] which could block the ion/electron transport channel and reduce the number of catalytic active sites. In contrast, in our case, the newly-produced 3D porous structures constructed from nanosheets will help to reduce the possible aggregation of materials on the electrode surface and prevent the above-mentioned adverse effect. It should be pointed out that direct phosphorization of CoNi-ZIF at 300 °C without involving the solvothermal treatment generates only irregularly shaped nanoparticles instead of ultrathin nanosheets in the final product of CoNi(20 : 1)-ZIF-P (Fig. S7, ESI†). Furthermore, TEM observation for an individual CoNi-P-NS (Fig. 2f) showed a discontinuous and rough surface with some tiny holes, which was quite different from the CoNi-NS with a continuous and smooth surface (Fig. 2e and Fig. S8, ESI†). The formation of in-plane pores is further supported by N_2 sorption measurements (Fig. S23, ESI†). This implies that the phosphorization treatment could "engrave" the sheet to engender more exposed surface area and active sites, beneficial for a high catalytic activity towards the OER. It is suggested that, when the MOFN templates were reacted with the PH_3, ligands of MOFNs were replaced by P atoms while creating some holes *in situ*. The detailed mechanism for the pore formation is still under study.

The crystal structure of CoNi-P-NS was analysed by high-resolution TEM (HRTEM) imaging. As shown in Fig. 2g, a well-resolved crystal lattice fringe spacing of 0.283 nm, corresponding to the (011) crystal plane of CoP, was observed. The corresponding selected area electron diffraction (SAED) pattern exhibits

bright rings with discrete spots, further testifying the crystalline character of CoNi-P-NS. The energy-dispersive X-ray (EDX) mapping analysis verifies the homogenous distribution of Co, Ni, and P within the whole nanosheet, along with a Co/Ni atomic ratio close to 20 : 1 and a P/total-metal-species atomic ratio close to 1 : 1 (Fig. 2h and Fig. S9, ESI†), which is supported by the results detected with an inductively coupled plasma atomic emission spectrometer (ICP-AES).

Fig. 3a shows the XRD patterns for the CoM-P-NS (see also Fig. S10, ESI†) with the characteristic diffraction peaks at 31.6°, 36.3°, 46.2°, 48.1°, 52.3° and 56.8° attributable to the (011), (111), (112), (211), (103), and (301) planes, respectively, of CoP (JCPDS-29-0497). Neither a new peak, possibly arising from other metal phosphides or impurities, nor a peak shift for the diffraction peaks of doped CoP, relative to the pristine CoP, was detected. These results unambiguously indicate that the secondary metal was indeed homogeneously intercalated into the crystal lattice of CoP and the effect of doping on the lattice constant became insignificant due to the similar ionic radius of the guest and host metal ions in the crystals.[36] Furthermore, X-ray photoelectron spectroscopy (XPS) was performed to monitor the surface chemistry (Fig. S11 and S12, ESI†). As can be seen in Fig. 3b, the high-resolution Co ($2p_{3/2}$) spectrum of CoNi-P-NS consists of component peaks at 778.3, 781.22, and 782.87 eV corresponding to CoP, oxidized cobalt species and cobalt hydroxide, respectively, which originate from surface oxidation.[37] The high-resolution P (2p) spectrum (Fig. 3c) can be deconvoluted into component peaks at 129.25 and 130.05 attributable to P ($2p_{3/2}$) and P ($2p_{1/2}$), respectively, from metal phosphides, along with one at 133.55 eV from oxidized phosphorus species due to the air exposure.[13] The high-resolution Ni ($2P_{3/2}$) spectrum (Fig. 3d) reveals component peaks at 852.80 eV corresponding to Ni–P as well as 856.50 and 861.76 eV arising from oxidized nickel species.[15,16] It is worth noting that the incorporation of Ni led to a negative shift in the binding energies of Co $2p_{3/2}$ and P $2p_{3/2}$ with respect to their counterpart for CoP, indicating that the intercalation of the second-metal indeed caused significant electronic modulation in the CoNi-P-NS homobimetallic phosphides[19] (*vide supra*).

By changing the molar ratio of Co/Ni in the starting precursor, we performed a series of control experiments to synthesize CoNi-P-NS materials with different Ni contents (Fig. S13–S17, ESI†). We noticed that it was not easy to produce multi-metallic phosphides without a segregated phase at a high Co/Ni ratio in the starting material (*e.g.* the molar ratio of Co/Ni $\geq$ 4 : 1) due to the phase separation caused by the lattice mismatch during the phosphorization process (Fig. S17, ESI†). It is noted that the composition of the Co and Ni starting precursors fails to affect the final sheet-like morphologies of the phosphides, suggesting the universality of our proposed synthetic protocol. Owing to the highly generic nature of the process shown in Fig. 1, however, our newly-developed approach could be considered as a general approach and was applied to the synthesis of other sheet-like monometallic and bimetallic phosphides, including CoMn-P-NS, CoCu-P-NS and CoZn-P-NS, from the corresponding ZIF and metal moieties (Fig. S18, ESI†). The morphologies, microstructures, and compositions for these bimetal phosphides were also thoroughly characterized (Fig. S4–S6, S10, S11 and S18, ESI†), showing that all the phosphides prepared by the general approach shown in Fig. 1 possess well-defined sheet-like structures with high composition homogeneity.

Having thoroughly characterised the CoM-P-NS, we investigated the electrocatalytic activity of CoM-P-NS supported by a glassy carbon electrode (GCE) for OER in alkaline media (1 M KOH) by using commercially available RuO_2 and 20 wt% Ir/C catalysts as references. As expected, compared to the pristine CoP-NS, the bimetallic phosphides showed significantly enhanced OER activity with the overpotential at 10 mA cm^{-2} reduced from 315 mV for the pristine CoP-NS to 273 mV for CoNi(20 : 1)-P-NS, 298 mV for CoMn(20 : 1)-P-NS, 281 mV for CoCu(20 : 1)-P-NS, and 276 mV for CoZn(20 : 1)-P-NS (Fig. 4a). We also prepared CoNi-P-NS catalysts with various Co/Ni ratios by using starting materials of different Co/Ni molar ratios, and found that the CoNi(20 : 1)-P-NS catalyst exhibited an optimized OER activity, while the decrease or increase of the Ni doping concentration resulted in the degeneration of the OER performance (Fig. S19, ESI†). Clearly, the OER activity of the available surface active sites can be effectively modulated by optimizing the elemental composition, creating a positive influence on the electrocatalytic ability. It is worth noting that the OER activity for CoNi(20 : 1)-P-NS with the homogenous single-phase is superior to that of the CoNi(4 : 1)-P-NS and CoNi(1 : 1)-P-NS samples with the segregated phase (Fig. S19, ESI†). This could be explained by the homogeneous single-phased CoNi(20 : 1)-P-NS favoring more effective 3d electronic modulation to achieve much stronger synergistic interplay between the two metal centres which promotes the OER performance.[21–24] As seen in Fig. 4c, d and Fig. S19–S22 (ESI†), among all the CoM-P-NS samples investigated in this study, the CoNi(20 : 1)-P-NS on GCE exhibited the lowest overpotential (273 mV) at 10 mA cm^{-2}, which was even lower than that of both the commercial RuO_2 (293 mV) and 20 wt% Ir/C (281 mV) catalysts with the same loading mass in 1.0 M KOH. Furthermore, the CoNi(20 : 1)-P-NS on GCE gives a much smaller tafel slope (45 mV dec^{-1}) relative to other samples such as Co-P-NS (80 mV dec^{-1}) and RuO_2 (81 mV dec^{-1}), indicating more favourable OER reaction kinetics. Given that the BET specific surface area (89.97 m^2 g^{-1}) for CoNi(20 : 1)-P-NS is similar to that of CoP-NS (94.49 m^2 g^{-1}, Fig. S23, ESI†), the specific activity of CoNi(20 : 1)-P-NS obtained by normalizing the OER current with the BET surface area is 0.375 mA cm_{BET}^{-2} at 1.55 V, about 5 times higher than that of CoP-NS (0.077 mA cm_{BET}^{-2}), indicating that the enhanced catalytic activity for CoNi(20 : 1)-P-NS is mainly due to the addition of the secondary metal.

To further improve the OER performance, we used a nickel foam (NF) to support the CoNi(20 : 1)-P-NS catalyst, as previously reported for other metallic catalysts.[19,24] The NF-supported CoNi(20 : 1)-P-NS catalyst exhibited a substantially enhanced OER catalytic activity, yielding an unexpectedly low overpotential of 209 mV with a small tafel slope of 52 mV dec^{-1}, over its GCE counterpart and even much better than most existing noble-metal-free alternatives for high performance OER catalysis (Table S1, ESI†) due to the excellent conductivity and electron

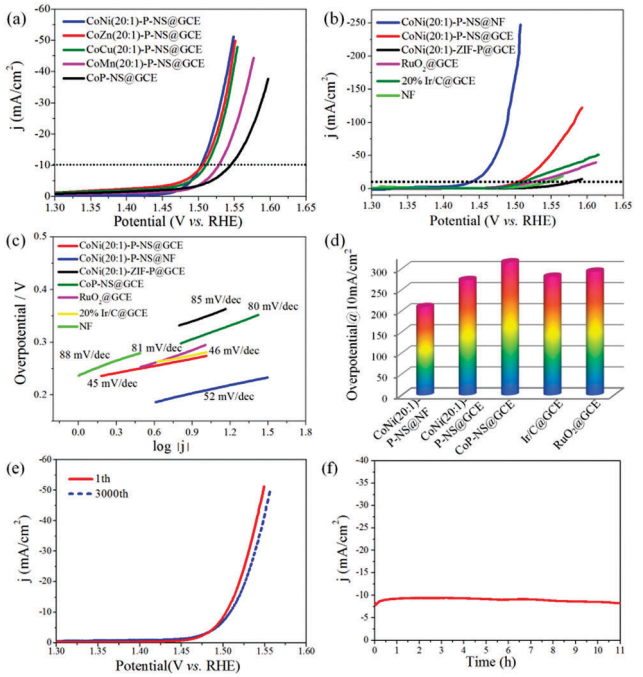

Fig. 4 Polarization curves of (a) CoP-NS and CoM(20 : 1)-P-NS (M = Ni, Mn, Cu, Zn), (b) CoNi(20 : 1)-P-NS on GCE or Ni foam (NF), CoNi(20 : 1)-ZIF-P, commercial 20% Ir/C and RuO_2 benchmarks, and Ni foam (all test were conducted in 1.0 M KOH); (c) Tafel plots derived from the corresponding polarization curves; (d) overpotential of CoNi(20 : 1)-P-NS on GCE or Ni foam (NF), CoP-NS, commercial 20% Ir/C and RuO_2 on GCE at the current density of 10 mA cm^{-2}; (e) polarization curves for CoNi(20 : 1)-P-NS on GCE initially (red) and after 3000 (blue) CV sweeps; (f) time-dependent current curve of CoNi(20 : 1)-P-NS measured at an applied overpotential of 280 mV at a rotation speed of 1600 rpm in 1.0 M KOH.

transfer ability of the metal foam substrates. To our knowledge, the observed OER performance is the best among the transition-metal-phosphide-based catalysts reported to date (Table S2, ESI†). Since CoNi(20 : 1)-P-NS@NF showed a much higher activity than the pristine NF (Fig. 4b and c), the enhancement in the OER performance for CoNi(20 : 1)-P-NS mainly arises from the bimetallic phosphides. Notably, the OER performance for CoNi(20 : 1)-P-NS is much better than that of the irregularly-shaped CoNi-P nanoparticles (CoNi(20 : 1)-ZIF-P, 348 mV at 10 mA cm^{-2}, 85 mV dec^{-1}, Fig. 4b and c) and recently reported CoMnP nanoparticles (330 mV at 10 mA cm^{-2}, 61 mV dec^{-1}),[21] and CoFeP nanorods (280 mV at 10 mA cm^{-2})[22] indicating particular advantages for the unique porous architecture assembled from 2D nanosheets. The stability of CoNi(20 : 1)-P-NS was tested by continuous cyclic voltammetry (CV) and linear sweep voltammetry (LSV) scanning for 3000 cycles in 1 M KOH at a scan rate of 50 mV s^{-1} (Fig. 4e and Fig. S21, ESI†); both show negligible change compared with their initial state. The time-dependent current density curve (Fig. 4f) under a static overpotential of 280 mV shows that the current density remains stable over 11 hours, further confirming the excellent long-term stability of CoNi(20 : 1)-P-NS.

To gain deep insight into the origin of the prominent OER activity in our bimetal phosphides, we performed density functional theory (DFT) calculations (Fig. 5). Previous computational studies have already demonstrated that the OER activities of transition metal compounds are mainly driven by the energetics of the OER intermediates (*OH, *O, and *OOH) on the catalyst surfaces.[38–41] Our computational results based on the pristine CoP (denoted as Co–P) show that the *OOH formation (ΔG_{*OOH} = 1.69 eV) is the rate-determining step (Fig. 5a and b). As pointed out in many previous studies, however, metal phosphides (*i.e.* CoP, Ni_2P) possess high sensitivity to air and their active surfaces become partially oxidized when exposed to air. As mentioned above, our XPS results also imply the existence of oxidized states, such as Co–O, P–O, and Ni–O species.[15,42] Thus, we used a model based on CoP with partial surface oxidation (denoted as Co–P–O) for the calculation, from which it is found that the binding energy of O reduced from 3.959 to 3.734 eV and the binding energy of OOH increased from 1.426 to 2.004 eV relative to the Co–P system (Fig. 5c). The above changes in binding energy are accompanied by a remarkable decrease in the free energy for the *OOH formation (ΔG_{*OOH} = 1.18 eV) and an increase in the free energy for the *O formation (ΔG_{*O} = 1.62 eV), which is regarded as the rate-determining step in the Co–P–O system. Similar to the Co–P–O system, our computational results

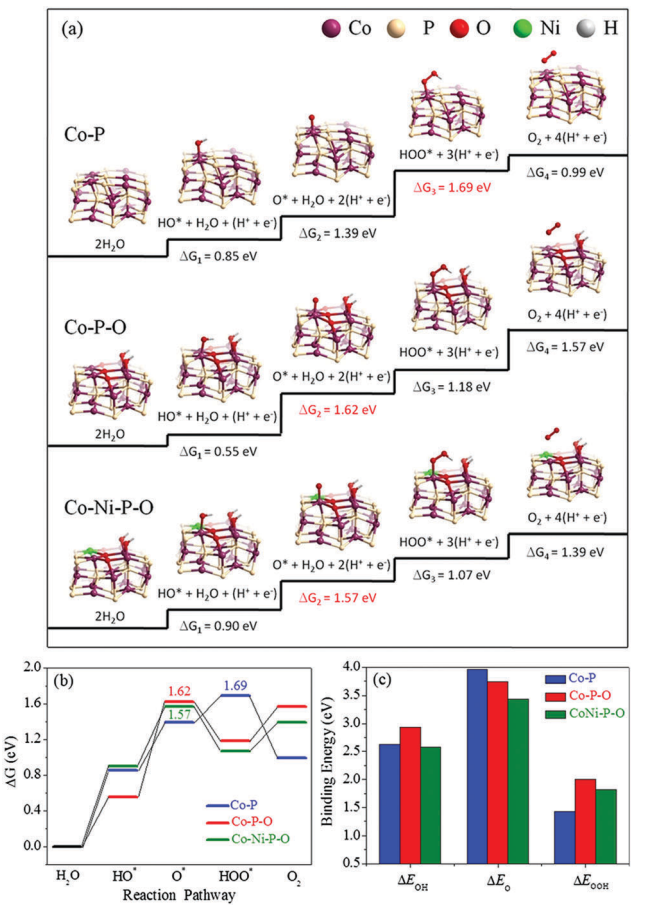

Fig. 5 (a and b) The corresponding primitive steps and standard free-energy diagram of the OER process on the pristine Co–P, partially oxidized CoP (Co–P–O) and Ni-doped CoP (Co–Ni–P–O) surfaces; (c) calculated binding energies of the OER intermediates on different active reaction sites.

for the surface oxidized CoNi-P (denoted as CoNi-P-O, Fig. 5a and b) reveal that, after the Ni doping, all the binding energies for OH, O and OOH decreased with respect to Co–P–O, leading to a decrease in the free energy of the rate-determining step (the *O formation ΔG_{*O} = 1.57 eV, Fig. 5a and b). It has been suggested that the presence of Ni could reduce the oxophilicity of Co, and thus engender a decrease in the binding energy of the intermediates on Co sites, when a Ni atom is in close proximity to a Co atom.[21] As expected, therefore, the CoNi-P catalyst can substantially lower the activation barrier relative to its monometal counterpart, as shown in Fig. 5a and b. The above results clearly indicate that homogenous Ni doping can effectively modulate the binding energies of the intermediates towards an optimal value to improve the energetics for the OER, benefiting O_2 evolution.

In comparison with previous reports,[21–23] our proposed MOFN-engaged approach represents a simple and promising strategy, which enables the effective regulation of the structure, composition, and electronics simultaneously. The remarkable OER activity of the newly-developed homobimetallic phosphide ultrathin nanosheets could be credited to the following aspects: (1) the agaric-like porous architecture as well as ultrathin sheet-like bimetallic phosphide building blocks with large surface area not only reduce the possible agglomeration of materials on the electrode surface and render highly exposed surface active sites, but also facilitate fast mass transport; (2) the in-plane holes created on the individual nanosheet surface render more exposed surface area and active sites; (3) homogeneous doping of a foreign metal with proper composition effectively tunes the electronic structure, thereby rendering optimal binding energies for OER intermediates due to the synergistic interplay between the host and guest metals; (4) the partially surface-oxidized metal species due to air exposure somewhat regulate the surface electronic structure to further improve the energetics of OER intermediates, as predicted by the aforementioned theoretical studies (Fig. 5).

Conclusions

In summary, we have, for the first time, established an effective and general approach to a new class of 2D Co-based homobimetallic phosphide nanosheets with single phase using MOFNs as the precursors *via* ion-assisted solvothermal treatment and low-temperature phosphorization. The newly-developed approach enabled the controlled transformation of bimetallic MOFNs into a series of corresponding bimetallic phosphides nanosheets (CoM-P-NS; M = Ni, Mn, Cu, Zn) with high composition homogeneity as well as a tunable Co/M ratio. The resulting bimetallic nanosheets were endowed with in-plane pores and interconnected with each other into agaric-like porous architectures, while secondary metals are homogeneously doped into the primitive CoP crystal lattice to effectively regulate the electronic structure and thereby lower the kinetic energy barrier for the OER, as revealed by our DFT calculations. As a result, our proposed strategy achieved synergistically structural, compositional, and electronic modulations, leading to the simultaneous improvement of the active sites and mass transport as well as the energetics for the OER. With the above benefits, the resulting CoM-P-NS showed dramatically improved OER performance with respect to monometallic CoP-NS and irregular bimetallic nanoparticles previously reported (Tables S1 and S2, ESI†). In particular, among the best reported transition-metal-phosphide electrocatalysts, the optimized CoNi(20 : 1)-P-NS electrocatalyst exhibited an unexpectedly low overpotential of 209 mV at 10 mA cm^{-2} in alkaline electrolyte, outperforming both the commercial RuO_2 and Ir/C benchmarks as well as most existing noble-metal-free electrocatalysts reported to date. The facile methodology developed in this study is highly general, which can be used for synthesizing various other 2D sheet-like monometallic and bimetallic compounds attractive for a variety of energy and environment-related applications. The proposed strategy of coordinated modulation is expected to broaden our horizons in designing novel highly-active electrocatalysts for various energy systems.

Acknowledgements

We gratefully acknowledge financial support from the Natural Science Foundation of China (No. 51573214, 21573066), the Youth 1000 Talent Program of China, the National Key Research and Development Program of China (No. 2016YFB0302301), and the National Postdoctoral Program for Innovative Talents (BX201600195).

Notes and references

1 N. S. Lewis and D. G. Nocera, *Proc. Natl. Acad. Sci. U. S. A.*, 2006, **103**, 15729–15735.
2 F. A. Frame, T. K. Townsend, R. L. Chamousis, E. M. Sabio, T. Dittrich, N. D. Browning and F. E. Osterloh, *J. Am. Chem. Soc.*, 2011, **133**, 7264–7267.
3 C. C. McCrory, S. Jung, J. C. Peters and T. F. Jaramillo, *J. Am. Chem. Soc.*, 2013, **135**, 16977–16987.
4 K. Gong, F. Du, Z. Xia, M. Durstock and L. Dai, *Science*, 2009, **323**, 760–764.
5 L. Dai, Y. Xue, L. Qu, H.-J. Choi and J.-B. Baek, *Chem. Rev.*, 2015, **115**(11), 4823–4892.
6 J. Zhang, L. Qu, G. Shi, J. Liu, J. Chen and L. Dai, *Angew. Chem., Int. Ed.*, 2016, **128**(6), 2270–2274.
7 D. Yu, E. Nagelli, F. Du and L. Dai, *J. Phys. Chem. Lett.*, 2010, **1**(14), 2165–2173.
8 J. Wang, W. Cui, Q. Liu, Z. Xing, A. M. Asiri and X. Sun, *Adv. Mater.*, 2016, **28**(2), 215–230.
9 M. W. Kanan, Y. Surendranath and D. G. Nocera, *Chem. Soc. Rev.*, 2009, **38**(1), 109–114.
10 P. Wang, F. Song, R. Amal, Y. H. Ng and X. Hu, *ChemSusChem*, 2016, **9**, 472.
11 E. J. Popczun, J. R. McKone, C. G. Read, A. J. Biacchi, A. M. Wiltrout, N. S. Lewis and R. E. Schaak, *J. Am. Chem. Soc.*, 2013, **135**(25), 9267–9270.
12 J. Tian, Q. Liu, A. M. Asiri and X. Sun, *J. Am. Chem. Soc.*, 2014, **136**(21), 7587–7590.

13 L. Jiao, Y.-X. Zhou and H.-L. Jiang, *Chem. Sci.*, 2016, **7**(3), 1690–1695.
14 B. You, N. Jiang, M. Sheng, S. Gul, J. Yano and Y. Sun, *Chem. Mater.*, 2015, **27**(22), 7636–7642.
15 L.-A. Stern, L. Feng, F. Song and X. Hu, *Energy Environ. Sci.*, 2015, **8**(8), 2347–2351.
16 A. Han, H. Chen, Z. Sun, J. Xu and P. Du, *Chem. Commun.*, 2015, **51**, 11626–11629.
17 J. Deng, P. Ren, D. Deng and X. Bao, *Angew. Chem., Int. Ed.*, 2015, **54**, 2100–2104.
18 J. Kibsgaard, C. Tsai, K. Chan, J. D. Benck, J. K. Nørskov, F. Abild-Pedersen and T. F. Jaramillo, *Energy Environ. Sci.*, 2015, **8**, 3022–3029.
19 Y. Tan, H. Wang, P. Liu, Y. Shen, C. Cheng, A. Hirata, T. Fujita, Z. Tang and M. Chen, *Energy Environ. Sci.*, 2016, **9**, 2257–2261.
20 Y. Li, H. Zhang, M. Jiang, Y. Kuang, X. Sun and X. Duan, *Nano Res.*, 2016, **9**, 2251–2259.
21 D. Li, H. Baydoun, C. N. Verani and S. L. Brock, *J. Am. Chem. Soc.*, 2016, **138**, 4006–4009.
22 A. Mendoza-Garcia, H. Zhu, Y. Yu, Q. Li, L. Zhou, D. Su, M. J. Kramer and S. Sun, *Angew. Chem., Int. Ed.*, 2015, **54**, 9642–9781.
23 A. Mendoza-Garcia, D. Su and S. Sun, *Nanoscale*, 2016, **8**, 3244–3247.
24 B. Zhang, X. Zheng, O. Voznyy, R. Comin, M. Bajdich, M. García-Melchor, L. Han, J. Xu, M. Liu, L. Zheng, F. P. García de Arquer, C. T. Dinh, F. Fan, M. Yuan, E. Yassitepe, N. Chen, T. Regier, P. Liu, Y. Li, P. De Luna, A. Janmohamed, H. L. Xin, H. Yang, A. Vojvodic and E. H. Sargent, *Science*, 2016, **352**, 333–337.
25 D. Yu, Q. Zhang and L. Dai, *J. Am. Chem. Soc.*, 2010, **132**, 15127–15129.
26 C. Zhu, D. Du, A. Eychmuller and Y. Lin, *Chem. Rev.*, 2015, **115**, 8896–8943.
27 D. Yu, E. Nagelli, R. Naik and L. Dai, *Angew. Chem., Int. Ed.*, 2011, **50**, 6575–6578.
28 S. Dou, L. Tao, J. Huo, S. Wang and L. Dai, *Energy Environ. Sci.*, 2016, **9**, 1320–1326.
29 D. Yu, Y. Yang, M. Durstock, J.-B. Baek and L. Dai, *ACS Nano*, 2010, **4**, 5633–5640.
30 X. J. Wu, X. Huang, J. Liu, H. Li, J. Yang, B. Li, W. Huang and H. Zhang, *Angew. Chem., Int. Ed.*, 2014, **53**, 5083–5187.
31 K. Xu, P. Chen, X. Li, C. Wu, Y. Guo, J. Zhao, X. Wu and Y. Xie, *Angew. Chem., Int. Ed.*, 2013, **52**, 10477–10481.
32 M. Chhowalla, Z. Liu and H. Zhang, *Chem. Soc. Rev.*, 2015, **44**, 2584–2586.
33 Q. H. Wang, K. Kalantar-Zadeh, A. Kis, J. N. Coleman and M. S. Strano, *Nat. Nanotechnol.*, 2012, **7**, 699–712.
34 K. S. Novoselov, A. K. Geim, S. V. Morozov, D. Jiang, Y. Zhang, S. V. Dubonos, I. V. Grigorieva and A. A. Firsov, *Science*, 2004, **306**, 666–669.
35 J. Yang, F. Zhang, H. Lu, X. Hong, H. Jiang, Y. Wu and Y. Li, *Angew. Chem., Int. Ed.*, 2015, **54**, 10889–10893.
36 Z. F. Huang, J. Song, K. Li, M. Tahir, Y. T. Wang, L. Pan, L. Wang, X. Zhang and J. J. Zou, *J. Am. Chem. Soc.*, 2016, **138**, 1359–1365.
37 Q. Liu, J. Tian, W. Cui, P. Jiang, N. Cheng, A. M. Asiri and X. Sun, *Angew. Chem., Int. Ed.*, 2014, **53**, 6710–6832.
38 J. Rossmeisl, Z. W. Qu, H. Zhu, G. J. Kroes and J. K. Nørskov, *J. Electroanal. Chem.*, 2007, **607**, 83–89.
39 Y. Jiao, Y. Zheng, M. Jaroniecb and S. Z. Qiao, *Chem. Soc. Rev.*, 2015, **44**, 2060–2086.
40 Y. Surendranath, M. W. Kanan and D. G. Nocera, *J. Am. Chem. Soc.*, 2010, **132**, 16501–16509.
41 J. Zhang, Z. Zhao, Z. Xia and L. Dai, *Nat. Nanotechnol.*, 2015, **10**, 444–452.
42 G.-F. Chen, T. Y. Ma, Z.-Q. Liu, N. Li, Y.-Z. Su, K. Davey and S.-Z. Qiao, *Adv. Funct. Mater.*, 2016, **26**, 3314–3323.